Journal of Electroanalytical Chemistry 818 (2018) 26–34

Contents lists available at ScienceDirect

Journal of Electroanalytical Chemistry

journal homepage: www.elsevier.com/locate/jelechem

Electrochemical synthesis of polyaniline-exfoliated graphene composite films and their capacitance properties

Abdelfetteh Sayah[a], Farid Habelhames[a,*], Ahmed Bahloul[a,*], Belkacem Nessark[a], Yvan Bonnassieux[b], Denis Tendelier[b], Mohamed El Jouad[c]

[a] Laboratory of Electrochemistry and Materials (LEM), Department of Engineering Process, Faculty of Technology, Ferhat Abbas University, Sétif-1 19000, Algeria
[b] Laboratory of Physics of Interfaces and Thin Films (LPICM), Ecole Polytechnique, CNRS/UMR 7647, 91128 Palaiseau, France
[c] Laboratory of Engineering Sciences for Energy (LabSIPE), National School of Applied Sciences, El Jadida 24002, Morocco

ARTICLE INFO

Keywords:
Graphene
Polyaniline
Chronoamperometry
Composite film
Specific capacitance

ABSTRACT

In this work, the graphene was synthesized by electrochemical exfoliation method, which was used to prepare the polyaniline-graphene composite film (PANI-GR) onto fluorine doped tin oxide (FTO) electrode by chronoamperometry technic at monomer oxidation potential 0.8 V vs. SCE. During the electropolymerization, the incorporation of the synthetized graphene into polyaniline matrix was assured by agitation of the electrolyte (10^{-2} M Ani/1 M H_2SO_4) containing different mass of graphene (1, 2 and 3 mg). By taking the advantages of the high conductivity of GR and the pseudocapacitance of PANI, the FTO/PANI-GR composite film was taken as an example for the application to the supercapacitor electrode materials. The morphology and structure of FTO/PANI and FTO/PANI-GR were characterized by different technics SEM, XRD, FTIR, Raman spectroscopy and UV–visible spectroscopy. The electrochemical performance was evaluated by cyclic voltammetry, galvanostatic charge-discharge tests and electrochemical impedance spectroscopy (EIS). The obtained specific capacitance for the PANI material alone is about 176.29 F g^{-1} this value was increased up to 305.57 F g^{-1} for the composite film PANI-GR 3 mg at 5 mV s^{-1}.

1. Introduction

Nowadays, conducting organic polymers are used in many technical applications especially in electrochemistry equipments like sensors, redox capacitors, catalysis and batteries [1–4]. Due to their high capacitance, conducting organic polymers represent the most important component of supercapacitor electrode [5,6]. Moreover, derivate carbon materials such active carbon [7], carbon nanotubes [8], and graphene [9–11] are known to be chemically stable and have large specific surface area. The latter features are so many targeted by searchers which that explain their use in supercapacitor electrodes. Thus, to produce high performance electrode materials, nano-composites conducting organic polymers and derivate carbon materials are undergoing deep investigations because of their interesting properties.

Within the same framework, graphene embodies a new element of carbon-based materials group represents the main constituent in several electrochemical devices such as supercapacitors. The expressed preference for the graphene is widely justified by its high electrical conductivity, mechanical strength, flexibility and effective working area [12]. The graphene witnesses significant stability during the charge–discharge process; however its specific capacitance (around 100–200 F g^{-1}) is proved to be limited by the stored energy mechanism mostly subsequent to the electric double-layer capacitance [13].

Among the processes leading to high quality graphene synthesis, the best way consist to proceed with direct exfoliation of graphite in solution, mainly electrochemical, sonochemical, and liquid-phase exfoliation [14–16]. In the opposite, the selected material rather required for pseudocapacitors, conducting organic polymers provides, in fact, high specific capacitance, nevertheless, they cause poor stability attributed to the Faradic mechanism [17]. In addition to the above-described characteristics, graphene may be combined with conducting organic polymer to form graphene/conducting organic polymer compound which is more electrochemically performant than pure graphene. The synergistic effects of each component that improve conductivity and increase electrochemical stability in the discharge process [18] explain the gain in performance shown by the graphene/conducting organic polymer. This stability as well as the high performance have been investigated in particular when combining conducting organic polymer with pure graphene such graphene/polyaniline [19–21], graphene/polypyrrole [22,23], and graphene/polythiophene composites

* Corresponding authors.
E-mail addresses: habelhamesfarid@yahoo.fr (F. Habelhames), ahmbahloul@yahoo.fr (A. Bahloul).

https://doi.org/10.1016/j.jelechem.2018.04.016
Received 26 April 2017; Received in revised form 7 April 2018; Accepted 9 April 2018
Available online 12 April 2018
1572-6657/

[24,25] particularly focused on. Among the conducting organic polymers, PANI, due to its cost relatively low, simple synthesis process and significant specific pseudocapacitance, has witnessed positive features towards active electrode materials pseudocapacitors [26].In the light of the exposed deductions and features, composites of graphene/polyaniline have acquired a major interest in the electrochemical field [27]. To recall the outlines of the process, in their first step starting electrochemical synthesis of graphene/PANI composite films with high capacitance of 640 $F g^{-1}$, at 0.1 $A g^{-1}$ [28]; Yan et al. produced a compound of graphene/polyaniline, in situ polymerization, with high specific capacitance of 1046 $F g^{-1}$ at a scan rate of 1 $mV s^{-1}$ relative to 115 $F g^{-1}$ for pure PANI [29], figures due to the presence of graphene nanosheets that modify the structure of PANI. Yan Jun and co-produced an effective supercapacitor electrode made of graphene nanosheets, carbon nanotubes and PANI, following an easy chemical in-situ mode. The electrode thus obtained is characterized by high specific capacitance 1035 $F g^{-1}$ at 1 $mV s^{-1}$ [30].

In the present study, we develop a new and a facile method to synthesis the polyaniline-graphene composite film, in one-step by electrochemical way. The graphene has been prepared by the electrochemical exfoliation method which was characterized by X-ray diffraction and FTIR spectroscopy. The (FTO/PANI-GR) composite films were electrochemically prepared by chronoamperometry technic on a working electrode (FTO) which was immersed in electrolyte containing the graphene dispersed by stirring at different weight (1, 2 and 3 mg) in sulphuric acid 1 M as the supporting electrolyte and 10^{-2} M aniline as monomer. The composite films are characterized by scanning electronic microscopy, FTIR spectroscopy, Raman spectroscopy and UV–visible spectroscopy. The capacitance properties were evaluated by cyclic voltammetry and electrochemical impedance spectroscopy.

2. Experimental

Graphene was synthesized by the electrochemical exfoliation. Two high-purity graphite rods, placed parallel with a separation of 6 cm in ionic solution. The ionic solution was prepared by diluting 2.6 ml of sulphuric acid (Sigma-Aldrich; 98%) in 100 mL of deionized water. The electrochemical exfoliation process was carried out by applying different potential between both graphite electrodes (5 V for 5 min). To prepare the graphene sheet suspension, the exfoliated graphene sheets were collected with a 100 nm porous filter and washed with deionized water by vacuum filtration. After drying, they were dispersed in N,N-diméthyl formamide DMF (Sigma-Aldrich) solution by mild water-bath sonication for 5 min. To remove unwanted large graphite particles produced in the exfoliation, the suspension was subjected to centrifugation at 2500 rpm. Then, the centrifuged suspension can be used for further characterizations and film preparation. All of these electrochemical exfoliation experiments were performed at room temperature.

Electrochemical tests were performed at room temperature in one compartment cell by the use a PGZ-301 Voltalab coupled with a computer equipped with software (voltamaster 4) which makes it possible to select the electrochemical technique and to fix the desired parameter. The electrochemical measurements were performed in a three-electrode cell, the working electrode is fluorine doped tin oxide glass substrate (FTO) (from SOLEMS), the reference electrode is a saturated calomel electrode (SCE) and the auxiliary electrode is a platinum plate.

The FTO/PANI and FTO/PANI-GR (1, 2 and 3 mg) films were characterized by various technics. The X-ray analysis was performed using a Rigaku make powder X-ray diffractometer (model RINT 2100) with a CuKα radiation (λ = 1.54 Å). The UV–visible spectrums of different films were recorded using a Shimadzu UV-1800 UV–vis spectrophotometer. The FTIR transmittance spectra of films were obtained using Fourier transform infrared spectrometer (IRAFFINITY-1S Shimadzu). Raman scattering measurements were recorded at room temperature with a HORIBA scientific Lab RAM HR Evolution RAMAN SPECTROMETER operating with a laser excitation source emitting at 437 nm. The Electric conductivity of the samples was measured using a Kheithley 2400 electrometer with LUCAS LABS Model (PR04-8400) Field emission scanning electron microscopy micrographs were obtained by using a (FESEM, JEOL, JSM-6701F).

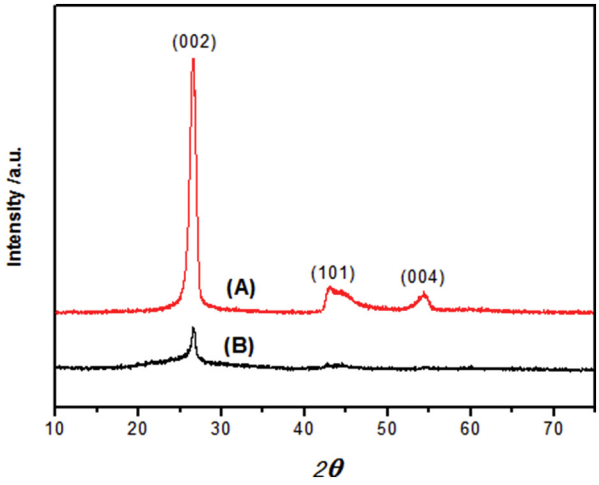

Fig. 1. XRD spectra of natural graphite (A) and graphene (B).

3. Results and discussion

The Fig. 1 represents the XRD patterns of graphite and graphene. So, in the XRD pattern of graphite powder (Fig. 1A) illustrates characteristics peaks of (002) at 26.50°, (101) at 42.31° and (004) at 54.60° with high intensity [31]. The powder of graphene (Fig. 1B) depicts a characteristic peak of (002) at 26.60° with weaker compared to graphite's peak. The decrease in the intensity of (002) plan peak indicates large exfoliation of graphite to graphene nanosheets [32]. The size of graphene nanoparticles estimation can be quantified by XRD in applying Debye–Scherrer's Eq. (1) as follows:

$$D = 0.9\lambda/w\cos\theta \quad (1)$$

where D is the size of nanoparticle, λ is the wavelength used for XRD, w is the full width half maxima and θ is the peak position, in applying this formula, we have calculated the size of nanoparticles of graphene as 13 nm.

The electropolymerization of aniline was carried out by chronoamperometry method from 10^{-2} M aniline dissolved in 1 M H_2SO_4, with in an imposed potential of 0.8 V vs. SCE for 180 s period of time. The graphene sheets was added into to the solution (1, 2 and 3 mg) and dispersed by stirring. Then the polyaniline-graphene composite was deposited on the working electrode after end time, all tests were realized in the same conditions as that imposed for electropolymerization of aniline in absence of the graphene.

Chronoamperograms of preparation of films composite FTO/PANI (A), FTO/PANI-GR 1 mg (B), 2 mg (C) and 3 mg (D) during electropolymerization were shown in Fig. 2. The obtained curves are very similar to that obtained by G. Zotti and al [33]. Through the initial stage, the anodic current slightly decreases and then increases with the square of the electrolysis time. The slight decrease in the current is attributed to the formation of a uniform polyaniline film through the radical-coupling polymerization [34].

In radical-coupling polymerization, the current is controlled by the diffusion of aniline, and a slight current decrease is observed. In addition, the charging current of the electric double layer was subtracted from the current for the polymerization. It is interesting to find that even after the initial stage the anodic current continues to increase with the electrolysis time. The nucleation processes correspond to the first stage and in the second stage correspond to two dimensional growth

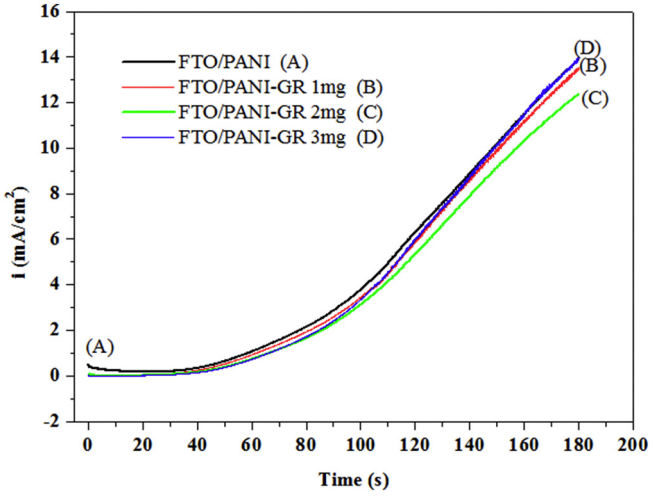

Fig. 2. Chronoamperograms of FTO/PANI (A), FTO/PANI-GR 1 mg (B), 2 mg (C) and 3 mg (D).

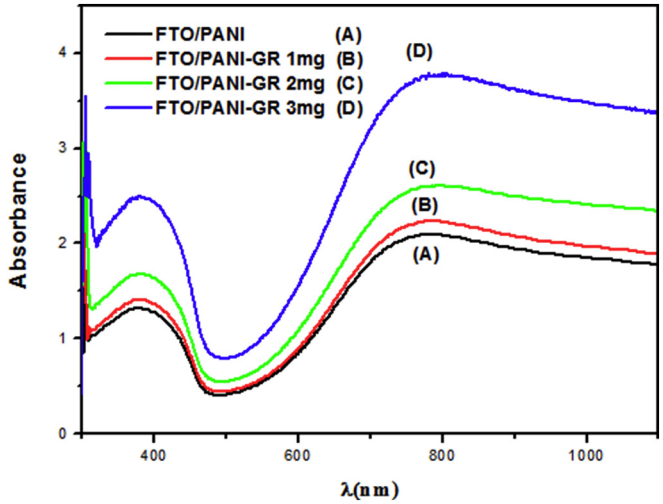

Fig. 4. UV–visible spectra of FTO/PANI (A), FTO/PANI-GR 1 mg (B), 2 mg (C) and 3 mg (D).

progressive nucleation and one-dimensional growth of progressive nucleation. The current response was fairly proportional to the time, in addition, the current/time slopes of the curves are proportional to the incorporated graphene weight.

The Fig. 3 shows the FESEM image of FTO/PANI and FTO/PANI-GR composite films. The Fig. 3A shows the FTO/PANI film that indicates a well porous morphology with distinct structures of uniform size. While the larger area stands for a close contact with the electrolyte. The outcome issues are proven to be in accordance with our earlier results [35].

From the SEM images observation, we can clearly perceive a noticeable change in the structure of FTO/PANI-GR shown in Fig. 3B compared to the film of FTO/PANI. The observed change imply that the graphene nanosheets have been embedded in PANI with adequate interconnections.

The UV–visible absorption spectra of FTO/PANI and FTO/PANI-GR (1, 2 and 3 mg) composite films are shown in Fig. 4. All the films presented two characteristic absorption bands at 395 nm and 790 nm wavelengths. The first absorption band is attributed to π–π* band transition, second absorption band is due to the formation of polaron or bipolaron states for charged defects in the polyaniline [36]. The absorption bands of composite films FTO/PANI-GR (1, 2 and 3 mg) increase gradually with the quantity of incorporated graphene, which show a bathochromic shift by comparing with FTO/PANI film, this is due to the fact that the presence of graphene particles ameliorate the electrical conductivity of PANI. Also, it can reveal an increase of the

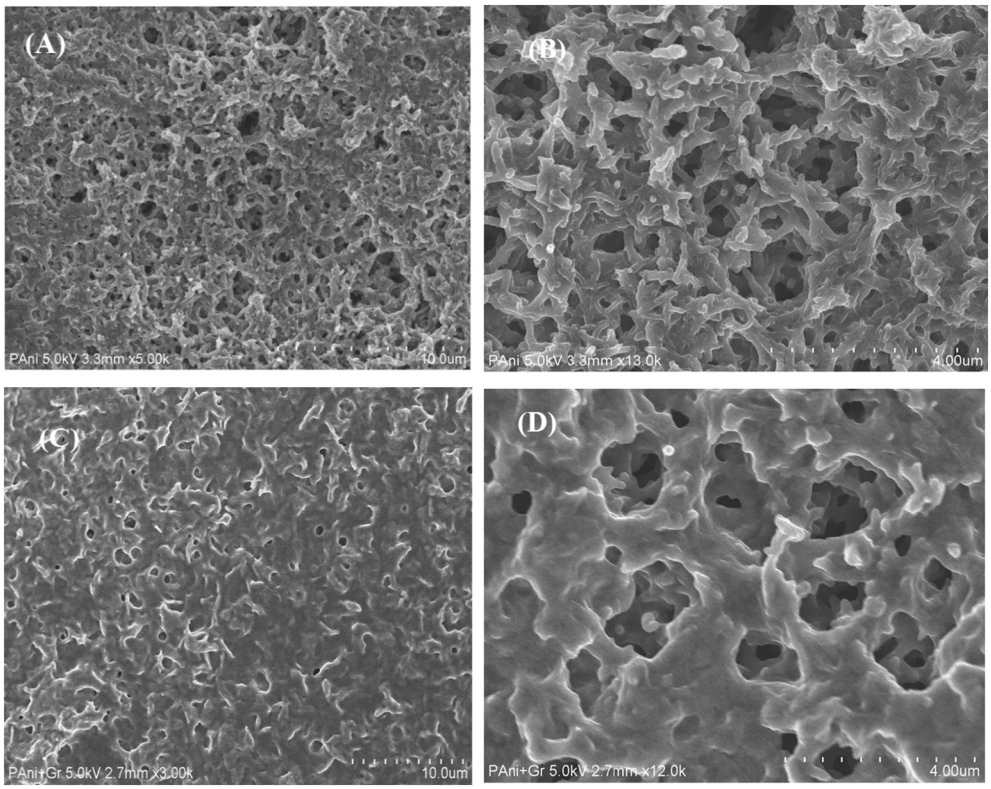

Fig. 3. FESEM images of FTO/PANI (A, B), FTO/PANI-GR (C, D).

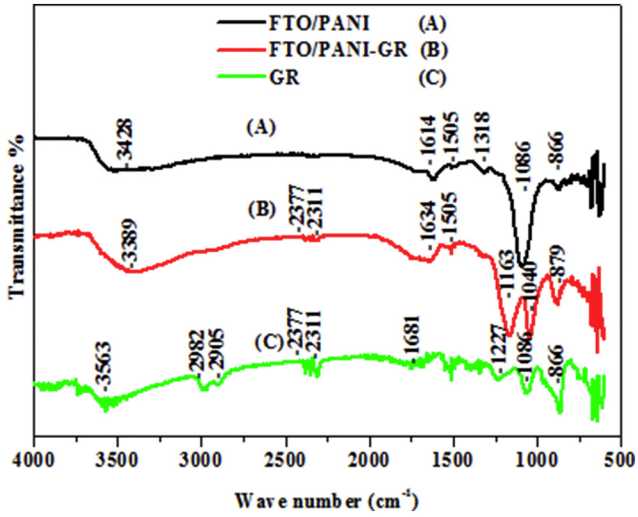

Fig. 5. FT-IR (ATR) spectrum of FTO/PANI (A), FTO/PANI-GR (B), GR (C).

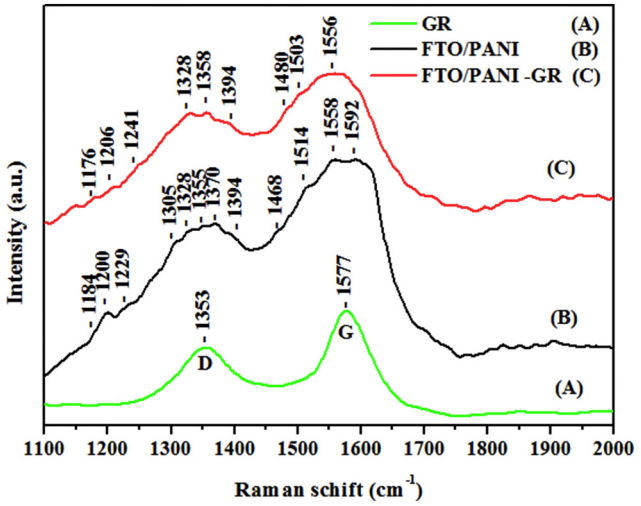

Fig. 6. Raman spectroscopy of GR (A), FTO/PANI (B), FTO/PANI-GR (C).

stability of the films upon incorporation of graphene in polyaniline matrix.

The Fig. 5 displays the FTIR spectra of FTO/PANI (A), FTO/PANI-GR (B) and graphene (C). The spectrum of polyaniline (Fig. 4A) displays different characteristic peaks involving the peaks at 866, 1086, 1318, 1505, 1614 and 3428 cm^{-1}. The peaks set correspond to the vibration modes as follow: bending of C—H out-of-plane on benzene ring (B), bending of C—H in-plane, mode of N = quinoid ring (Q)=N, stretching of aromatic-N, stretching of N—B—N, stretching of N=Q=N, and the peak at 3428 cm^{-1} was due to O—H stretching band of water, respectively [37,38].

Through the comparison of the two spectra sets, FTO/PANI-GR (Fig. 4B) to FTO/PANI, we notice an occurrence of a band at 1040 cm^{-1}. The new band in vibration absorption mode stands for a charge transfer and specific interaction of graphene fragments with quinoid rings of PANI skeleton [39].

The Fig. 5C displays the spectrum of pure graphene pointing up to a C=C characteristic peaks of graphene materials within the range 1340–1700 cm^{-1}. The issued spectrum reveals an absorption peak at 1227 cm^{-1} that refers to the C—OH stretching. In addition, a peaks at 2982 and 2905 cm^{-1} refers to the C—H stretching vibrations. Finally, the first peaks displayed at 1681 cm^{-1} is related to the stretching vibration of carboxylic group and the second peaks displayed at 1086 cm^{-1} is assigned to the C—O stretching vibrations [40].

Raman spectra of graphene (A), FTO/PANI (B) and FTO/PANI-GR (C) are shown in Fig. 6. The graphene spectrum 6A depict two large bands, the G-band at 1353 cm^{-1} representing the in-plane bond-stretching motion of the pairs of sp^2 carbon atoms (E_2g) and the D-band at 1577 cm^{-1}corresponding to in-plane (A_1g) zone-edge mode, is inherently Raman-active at the graphitic edges [29,41]. The D-band is significantly less intense than the G-band; it means the graphene structure contains low amount of defects and low impurities [42].

The FTO/PANI spectrum 6B shows the C—C stretching of the benzenoid ring band at 1592 cm^{-1}, the C=C stretching of the quinoid ring at 1558 cm^{-1}, the C=N stretching of the quinoid ring at 1514 cm^{-1}, the C—C stretching of the quinoid ring at 1468 cm^{-1}, the C—N stretching of the quinoid ring at 1355 cm^{-1}, the C—N stretching of the benzenoid ring at 1200 cm^{-1} and the C—H bending of the benzenoid ring at 1184 cm^{-1} [43,44].

The FTO/PANI-GR spectrum 6C exhibits all bands representing graphene and polyaniline. It confirms the interaction of graphene with the polymer matrix quinoidal structure via π–π stacking. Accordingly, all large bands arrays intensity remarkably decreases and the polyaniline bands slightly shift [29,42].

Cyclic voltammetry is an ideal technic for characterizing the capacitive performance of materials in supercapacitors. Fig. 7 shows the cyclic voltammograms of FTO/PANI and FTO/PANI-GR (1, 2 and 3 mg) composite films carried out in a potential range of −0.2 to 1 V vs. SCE at different scan rates (5, 10, 20, 30, 50 mV s^{-1}). All the cyclic plots show a reversible redox response.

First, in comparison with the FTO/PANI film, we observe all FTO/PANI-GR composite films show a significant increase in the areas of the charge and discharge curves in the cyclic voltammetry plots, which increase with increasing the graphene mass incorporated in polymer matrix. Secondly, three pairs of redox peaks are observed. The two pairs of peaks at 0.2 and 0.8 V vs. SCE are associated with the redox of PANI molecules from its semiconducting state (leucoemeraldine) to its conductive from (emeraldine) and emeraldine to its full oxidation state (pernigraniline) respectively [45]. Meanwhile, the weak peaks at 0.4–0.5 V V vs. SCE are attributed to the formation of the head-to-tail dimer [46]. Third, we can observe that in increasing the potential scan rate, the anodic peaks shift positively and the cathodic peaks shift negatively. This phenomenon is attributed to the increase in the resistance of the electrode. Meanwhile, the peak current increases steadily with the increase of potential scan rate, indicating a good rate capability of composite films.

The high cyclic voltammetry response currents is observed for the FTO/PANI-GR 3 mg composite film which show significantly higher specific capacitance than FTO/PANI, this is due to the porosity structure of the FTO/PANI-GR composite films than FTO/PANI film and due to the pseudocapacitance of polyaniline. The FTO/PANI-GR composite films electrodes integrate the excellent electrical conductivity with the high pseudocapacitance of PANI, thus allowing an enhanced electrocapacitive performance. It is given that the pseudocapacitance of PANI comes from the surface faradic redox reaction, PANI with a large electrochemical active surface area would be highly desirable to maximize its utilization efficiency [47,48]. Although the high conductivity of graphene improves the conductivity of PANI, as the presence of graphene nanosheets provide a high contact interface between PANI and electrolyte [44,49,50] consequently, exploration of graphene with high surface area and open. So the specific capacitance is calculated accurately on the basis of the following Eq. (2):

$$SC = \frac{\int_{E_1}^{E_2} i(E)\, dE}{2\,(E_1 - E_2)\, mv} \quad (2)$$

SC: specific capacitance

E_2-E_1: potential window in cyclic voltammetry

$\int_{E_1}^{E_2} i(E)\, dE$: voltammetric charge obtained by integration of curve

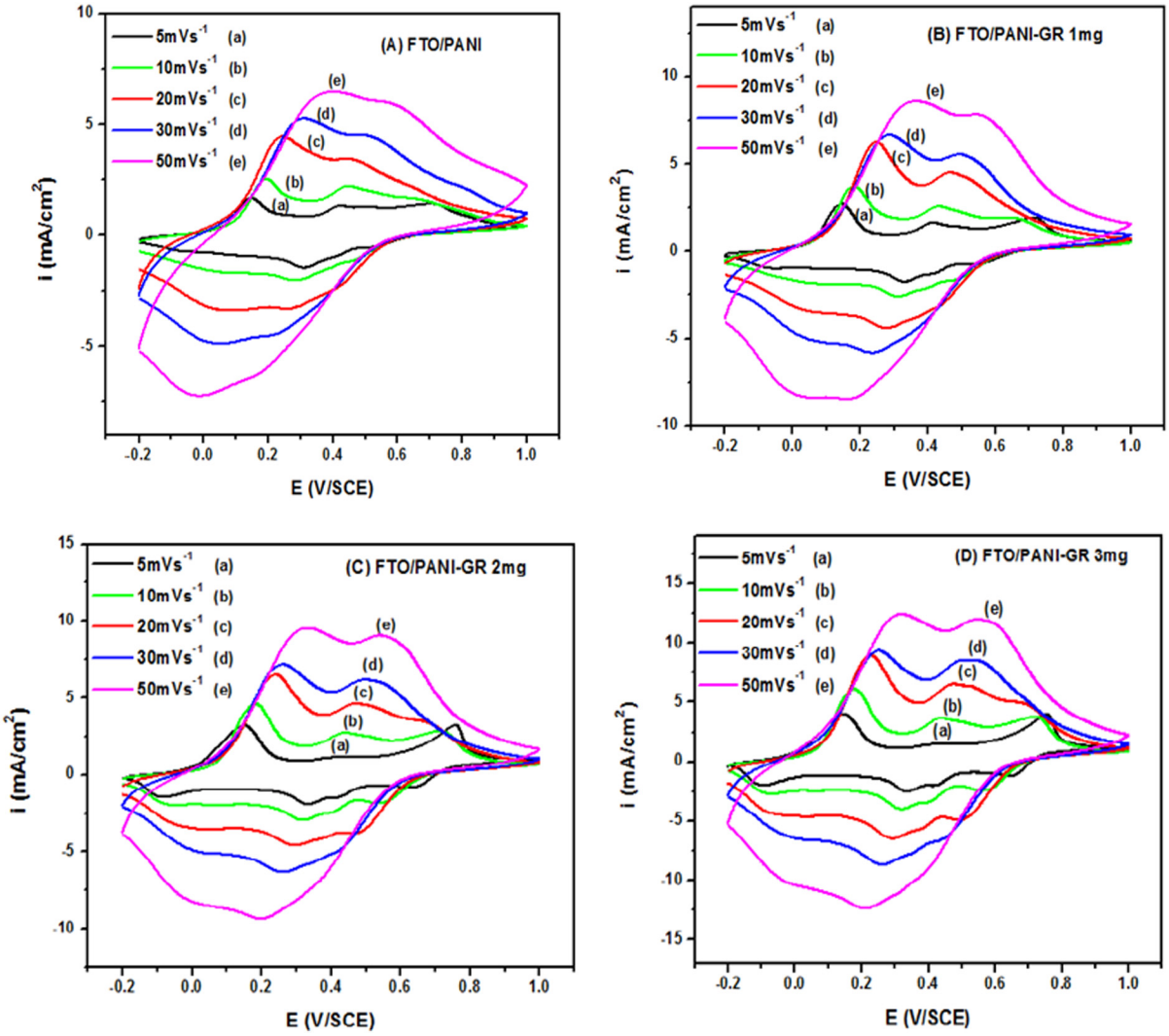

Fig. 7. Cyclic voltammograms of FTO/PANI (A), FTO/PANI-GR 1 mg (B), 2 mg (C) and 3 mg (D), at different scan rates in 1 M H_2SO_4 electrolyte.

in CV

m: weight of deposited materiel on working electrode, we used a balance with accuracy of 0.01 mg

v: scan rate.

The specific capacitances of FTO/PANI and FTO/PANI-GR (1, 2 and 3 mg) composite films in dependence of different scan rates are illustrated in Fig. 8. The FTO/PANI film show a specific capacity of about 176.29 F g^{-1} at 5 mV s^{-1}, after the incorporation of the graphene sheets, we have observed a significant increase in specific capacitance which were 201.34, 274.56, and 305.57 F g^{-1} for FTO/PANI-GR (1, 2 and 3 mg) composite films respectively.

However, the FTO/PANI film present the worse rate capability, their specific capacitance shows different extents of decrease with increasing the potential scan rate. The FTO/PANI-GR 3 mg composite film shown the best rate capability, this may be attributed to the presence of the graphene in polymer matrix, which allows the fast and efficient electron and ion transport in the electrode surface.

The impedance spectra of FTO/PANI and FTO/PANI-GR 1 mg (B), 2 mg (C) and 3 mg (D) composite films measured at open circuit potential (0.230 V vs. SCE) is shown as Nyquist diagrams in Fig. 9. The films were analyzed in aqueous solution 1 M H_2SO_4. All measurements were plotted on a frequency band ranging between 100 KHz and 100 MHz, with an alternative current voltage of 10 mV.

The EIS measurements are interpreted in terms of an equivalent electric circuit, the electrode/solution interface is modelled as a circuit

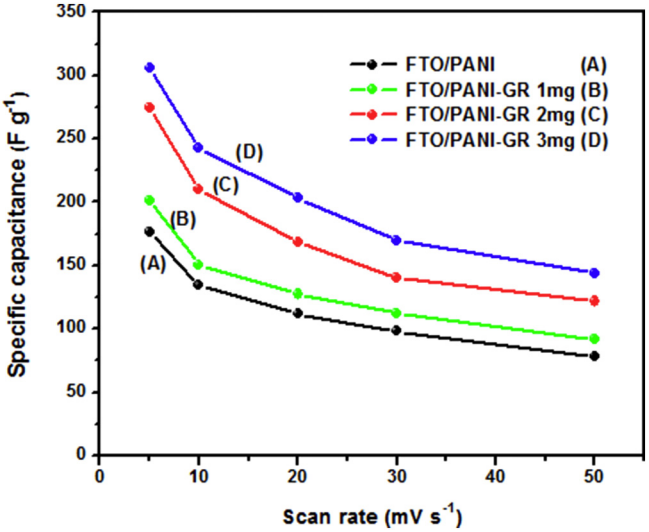

Fig. 8. Specific capacitances of FTO/PANI (A), FTO/PANI-GR 1 mg (B), 2 mg (C) and 3 mg (D), at different scan rates.

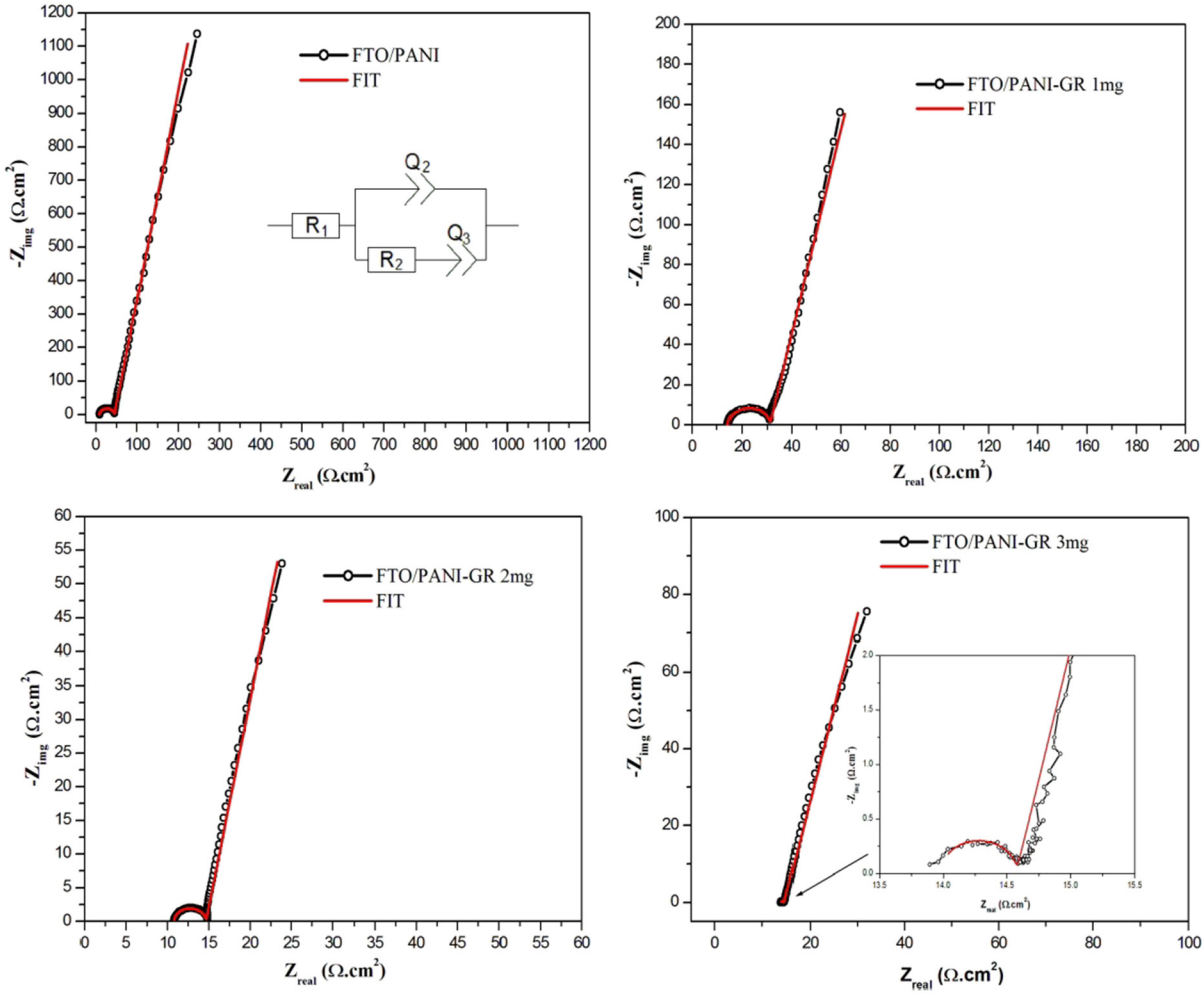

Fig. 9. Nyquist diagrams fitting of FTO/PANI and FTO/PANI–GR with different mass, obtained at OCV in 1 M H_2SO_4.

composed of a constant phase element (Q_2) in parallel of charge transfer resistance (R_2) and another constant phase element (Q_3); this circuit is preceded by an electrolyte resistance (R_1). The fitting of the a.c. impedance data was done using electrochemical software the EC-Lab Z fitting.

As can be seen, the EIS spectra have a single semicircle in the high frequency region characteristic of a charge transfer process and a straight line with a high slope which approaches a 90° in a low-frequency region indicates a capacitive behavior. The straight line with a high slope at the low frequency region can confirm that these composite films can be used as electrodes in capacitors [51].

The semicircle diameter decreases with increasing graphene content in polyaniline matrix, suggesting a decrease in resistance and therefore a significant increase in the electric conductivity of composite films containing graphene, from 35.88 Ω·cm^2 for FTO/PANI to 16.76 Ω·cm^2 for FTO/PANI-GR 1 mg, 3.88 Ω·cm^2 for FTO/PANI-GR 2 mg and 0.59 Ω·cm^2 for FTO/PANI-GR 3 mg. These results indicate that a slower electron transfer in PANI film, but the incorporation of graphene nanosheets in PANI film can improve the interaction between conductive polymer chains. The errors of all parameters are from 0.1% to 7.8%, indicating that these fitting values are acceptable (Table 1).

The usefulness of EIS is a good tool to estimate the specific capacitance of different films by combining electrical double-layer capacitance (Q_2) producing on the surface of the film and pseudocapacitance (Q_3) of the film. The value of Q_2 is much less than that of Q_3, so the specific capacitances of films are regarded to be the value of Q_3 approximately. The estimated specific capacitance is 41.09 F·g^{-1} for FTO/PANI, 41.88 F·g^{-1} for FTO/PANI-GR 1 mg, 62.05 F·g^{-1} for FTO/PANI-GR 2 mg and 66.2 F·g^{-1} for FTO/PANI-GR 3 mg. The results indicate that the conductivity of the film affect on the value of the capacitance.

The specific capacitance can be also estimated by EIS technic at a specific frequency by calculating of the real (C′) and imaginary (C″) capacitances, the Fig. 10 shows C′ and C″ vs logarithm frequency curves carried out at 1 V/SCE. These parameters were given by the Eqs. (3) and (4):

$$C' = -Z''/w\,|Z|^2 \quad (3)$$

$$C'' = Z'/w\,|Z|^2 \quad (4)$$

and then, the specific capacitance was calculated by the Eq. (5):

$$|C| = [(C')^2 + (C'')^2]^{1/2} \quad (5)$$

The obtained specific capacitances by EIS were 15.21, 22.57, 31.93 and 106.34 F g^{-1} for FTO/PANI-GR (1, 2 and 3 mg) composite films respectively.

The capacitance propriety can be described as relaxation time constant (τ_0) at frequency (f_0), which clearly defines the boundary between the resistive and capacitive behaviors in imaginary frequency component C″ vs frequency plot [52]. Here, the relaxation time constant (τ_0) values are 111.72 ms for PANI and 107.51 ms for PANI + GR 3 mg, which clearly indicates that the presence of graphene in polymer matrix let a fast charge transport phenomena than PANI alone.

The Fig. 11 displays the electric conductivity of the FTO/PANI/graphene composite where the graphene amount us added gradually.

The electric conductivity of FTO/PANI and FTO/PANI-GR (1, 2 and

Table 1
Impedance electrical parameter values corresponding to FTO/PANI, FTO/PANI-GR 1, 2 and 3 mg.

Element	FTO/PANI		FTO/PANI-GR 1 mg		FTO/PANI-GR 2 mg		FTO/PANI-GR 3 mg	
	Value	err.%	Value	err.%	Value	err.%	Value	err.%
R_1 ($\Omega \cdot cm^2$)	**2.59**	0.3	**4.00**	0.4	**3.02**	0.3	**3.91**	0.2
R_2 ($\Omega \cdot cm^2$)	**35.88**	0.6	**16.76**	1.4	**3.884**	4.6	**0.598**	6.2
Q_2 ($\mu F \cdot cm^2$)	**66.22**	3.4	**64.06**	1.4	**43.29**	2.3	**20.6**	7.8
n_2	**0.99**	0.4	**0.98**	1	**1**	0.2	**1**	1.1
Q_3 ($F \cdot g^{-1}$)	**41.09**	0.4	**41.88**	0.6	**62.05**	0.5	**66.2**	0.3
n_3	**0.9**	0.2	**0.85**	0.4	**0.9**	0.3	**0.87**	0.1

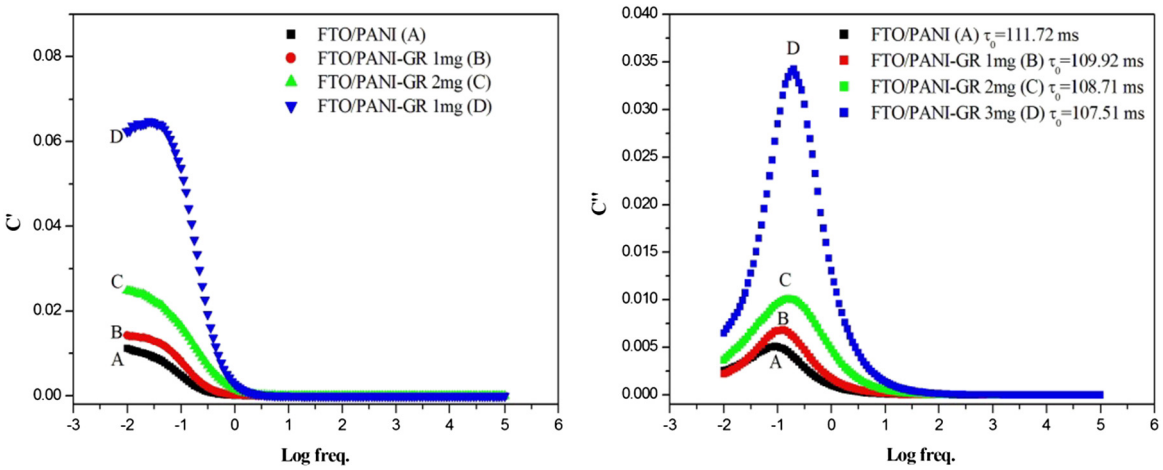

Fig. 10. The real (C′) and imaginary (C″) capacitances vs logarithm frequency curves at 1 V/SCE.

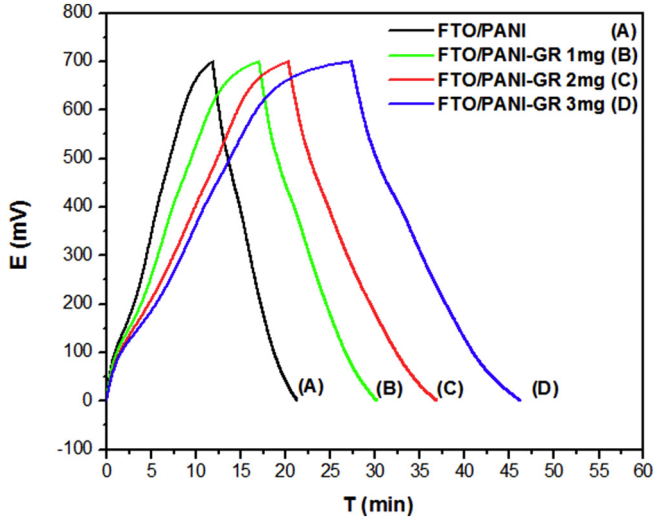

Fig. 11. Galvanostatic charge-discharge curves of FTO/PANI (A), FTO/PANI-GR 1 mg (B), 2 mg (C) and 3 mg (D) at the current density of 0.1 $A \cdot g^{-1}$ in 1 M H_2SO_4 from 0 to 0.7 V.

Table 2
Electric conductivity of FTO/PANI and FTO/PANI-GR (1, 2 and 3 mg) composite films.

	FTO/PANI	FTO/PANI-GR 1 mg	FTO/PANI-GR 2 mg	FTO/PANI-GR 3 mg
Electrical conductivity (S/cm)	0.09	0.454	4	4.76

3 mg) composite films measured are reported in Table 2. Systematically, the electric conductivity of FTO/PANI-GR composite films increased with the increase of the graphene amount in polymer film. The conductivity attained the value of 4.76 S/cm for FTO/PANI-GR 3 mg which is fifty times higher than the conductivity of the pure FTO/PANI 0.09 S/cm. The noticed electric conductivity increase is likely due to two facts: the first is the nanoscale dispersion of graphene nanosheets in the PANI matrix with formation of conducting network while the second is the interaction between the big π-conjugated structure of the graphene and the quinoid ring of PANI, where the graphene within the PANI matrix served as electric conductive bridge [53].

The electrochemical performance of the FTO/PANI (A), FTO/PANI-GR 1 mg (B), 2 mg (C) and 3 mg (D)in asymmetric supercapacitor with tow electrodes was investigated by the galvanostatic charging-discharging measurements in 1 M H_2SO_4. A typical charge discharge profiles was observed at 0,1 $A \cdot g^{-1}$were shown in Fig. 11, all curves indicated nearly triangular shaped linear charge-discharge profile over the measured potential limit between 0 and 0.7 V, which confirm the capacitive characteristics of the electrodes. In order, to estimate the specific capacitance (SC) from discharge curves, we have used this Eq. (6):

$$SC = It/m\Delta V \quad (6)$$

where I is the charge/discharge current, t is discharge time, ΔV is the potential limit during discharge and m is the weight. The specific capacitance of the electrodes was found to be 80.74 F g^{-1} for FTO/PANI and 104.05 F g^{-1}, 142.37 F g^{-1}, 162 F g^{-1} for FTO/PANI-GR 1, 2, 3 mg respectively. It can be observed that an important increase in the specific capacitance of about 100%. This result further supports the specific capacitance observed from the cyclic voltammetry measurements.

The electrochemical performance of the supercapacitor is an important factor for practical applications. Therefore, the energy and power density of the materials in asymmetric supercapacitor with two

electrodes system were calculated after galvanostatic charge/discharge test at 0.1 A g^{-1}. In the case of FTO/PANI electrode, the observed energy density was no higher than 5.49 Wh kg^{-1} with 34.95 W kg^{-1} as power outcome. But in presence of graphene in material electrode, the energy density proved to be higher than FTO/PANI electrode that was about of 7.08 Wh kg^{-1} for FTO/PANI-GR 1 mg, 9.68 Wh kg^{-1} for FTO/PANI-GR 2 mg and 11.02 Wh kg^{-1} for FTO/PANI-GR 3 g. The obtained power at low current 0.1 A g^{-1} was 35.04 W kg^{-1}, 35.1 W kg^{-1} and 35.2 W kg^{-1} for FTO/PANI-GR 1, 2 and 3 mg, respectively. The energy and power performance values of materials containing graphene are fairly better than the polyaniline alone.

4. Conclusion

In summary, the (FTO/PANI-GR) composite films were electrochemically prepared by chronoamperometry technic on a working electrode (FTO) which was immersed in electrolyte containing the graphene dispersed by stirring at different weight (1, 2 and 3 mg) in sulphuric acid 1 M as the supporting electrolyte and 10^{-2} M aniline as monomer. The FTO/PANI-GR composite films were taken as an example for the application to the supercapacitor electrode materials. The obtained specific capacity for the PANI material alone is about 176.29 F g^{-1} this value was increased up to 305.57 F g^{-1} for the composite film FTO/PANI-GR 3 mg at 5 mV s^{-1}. While the films with polyaniline and graphene give a good capacitance, this is due to the beneficial effect of graphene electronic conductivity.

References

[1] H.T. Hie, H.T. Giang, T. Trung, C.V. Tuan, Enhancement of biosensing performance using a polyaniline/multiwalled carbon nanotubes nanocomposite, J. Mater. Sci. 52 (2017) 1694–1703, http://dx.doi.org/10.1007/s10853-016-0461-z.

[2] A. Bahloul, B. Nessark, E. Briot, H. Groult, A. Mauger, K. Zaghib, C.M. Julien, Polypyrrole-covered MnO_2 as electrode material for supercapacitor, J. Power Sources 240 (2013) 267–272, http://dx.doi.org/10.1016/j.jpowsour.2013.04.013.

[3] L. Gu, J. Wang, R. Qi, X. Wang, P. Xu, X.A. Han, Novel incorporating style of polyaniline/TiO_2 composites as effective visible photocatalysts, J. Mol. Catal. A Chem. 357 (2012) 19–25, http://dx.doi.org/10.1016/j.jpowsour.2013.04.013.

[4] H. Mi, F. Li, Ch. He, X. Chai, Q. Zhang, Y. Li, J. Liu, Three-dimensional network structure of silicon-graphene-polyaniline composites as high performance anodes for Lithium-ion batteries, Electrochim. Acta 190 (2016) 1032–1040, http://dx.doi.org/10.1016/j.electacta.2015.12.182.

[5] G. Li, Y. Li, H. Peng, Y. Qin, Synthesis and electrochemical performances of dispersible polyaniline/sulfonated graphene composite nanosheets, Synth. Met. 184 (2013) 10–15, http://dx.doi.org/10.1016/j.synthmet.2013.09.016.

[6] J. Xu, K. Wang, Z. Zu, B.H. Han, Z. Wei, Hierarchical nanocomposites of polyaniline nanowire arrays on graphene oxide sheets with synergistic effect for energy storage, ACS Nano 4 (2010) 5019–5026, http://dx.doi.org/10.1021/nn1006539.

[7] L. Li, E. Liu, J. Li, Y. Yang, H. Shen, Z. Huang, X. Xiang, W. Li, A doped activated carbon prepared from polyaniline for high performance supercapacitors, J. Power Sources 195 (2010) 1516–1521, http://dx.doi.org/10.1016/j.jpowsour.2009.09.016.

[8] L. Deng, R.J. Young, I.A. Kinloch, A.M. Abdelkader, S.M. Holmes, D.A. De Haro-Del Rio, S.J. Eichhorn, Supercapacitance from cellulose and carbon nanotube nanocomposite fibers, ACS Appl. Mater. Interfaces 5 (2013) 9983–9990, http://dx.doi.org/10.1021/am403622v.

[9] S.Z. Wu, W. Ren, D.W. Wang, F. Li, B. Liu, H.M. Cheng, High-energy MnO_2 nanowire/graphene and graphene asymmetric electrochemical capacitors, ACS Nano 4 (2010) 5835–5842, http://dx.doi.org/10.1021/nn101754k.

[10] B. Zhang, Y. Chen, Y. Ren, L.Q. Xu, G. Liu, E.T. Kang, Ch. Wang, Ch.X. Zhu, K.G. Neohet, In situ synthesis and nonvolatile rewritable-memory effect of polyaniline-functionalized graphene oxide, J. Chem. Eur. 19 (2013) 6265–6273, http://dx.doi.org/10.1002/chem.201203940.

[11] Z. Wen, X. Wang, S. Mao, Z. Bo, H. Kim, S. Cui, G. Lu, X. Feng, Crumpled nitrogen-doped graphene nanosheets with ultrahigh pore volume for high-performance supercapacitor, J. Chem. Adv. Mater. 24 (2012) 5610–5616, http://dx.doi.org/10.1002/adma.201201920.

[12] M. Jing, C. Wang, H. Hou, Z. Wu, Y. Zhu, Y. Yang, X. Jia, Y. Zhang, X. Ji, Ultrafine nickel oxide quantum dots embedded with few-layer exfoliative graphene for an asymmetric supercapacitor: enhanced capacitances by alternating voltage, J. Power Sources 298 (2015) 241–248, http://dx.doi.org/10.1016/j.jpowsour.2015.08.039.

[13] F. Liu, S. Song, D. Xue, H. Zhang, Folded structured graphene paper for high performance electrode materials, Adv. Mater. 24 (2012) 1089–1094, http://dx.doi.org/10.1002/adma.201104691.

[14] J. Wang, K.K. Manga, Q. Bao, K.P. Loh, High-yield, synthesis of few-layer graphene flakes through electrochemical expansion of graphite in propylene carbonate electrolyte, J. Am. Chem. Soc. 133 (2011) 8888–8891, http://dx.doi.org/10.1021/ja203725d.

[15] C.Y. Su, A.Y. Lu, Y. Xu, F.R. Chen, A.N. Khlobystov, L.J. Li, High-quality thin graphene films from fast electrochemical exfoliation, ACS Nano 5 (2011) 2332–2339, http://dx.doi.org/10.1021/nn200025p.

[16] H. Xu, K.S. Suslick, Sonochemical preparation of functionalized graphenes, J. Am. Chem. Soc. 133 (2011) 9148–9151, http://dx.doi.org/10.1021/ja200883z.

[17] C. Liu, F. Li, L.P. Ma, H.M. Cheng, Advanced materials for energy storage, Adv. Mater. 22 (2010) E28–E62, http://dx.doi.org/10.1002/adma.200903328.

[18] Y. Liu, Y. Ma, S. Guang, H. Xu, X. Su, Facile fabrication of three-dimensional highly ordered structural polyaniline–graphene bulk hybrid materials for high performance supercapacitor electrodes, J. Mater. Chem. A 2 (2014) 813–823, http://dx.doi.org/10.1039/c3ta13513f.

[19] W. Xinming, W. Qiguan, Z. Wenzhi, W. Yan, C. Weixing, Enhanced electrochemical performance of hydrogen-bonded graphene/polyaniline for electrochromo-supercapacitor, J. Mater. Sci. 51 (2016) 7731–7741, http://dx.doi.org/10.1007/s10853-016-0055-9.

[20] P. Kumari, K.K. Khawas, S. Nandy, B.K. Kuila, A supramolecular approach to polyaniline graphene nanohybrid with three dimensional pillar structures for high performing electrochemical supercapacitor applications, Electrochem. Acta. 190 (2016) 596–604, http://dx.doi.org/10.1016/j.electacta.2015.12.130.

[21] Z.F. Li, H.Y. Zhang, Q. Liu, L.L. Sun, L. Stanciu, J. Xie, Fabrication of high-–surface–area graphene/polyaniline nanocomposites and their application in supercapacitors, ACS Appl. Mater. Interfaces 5 (2013) 2685–2691, http://dx.doi.org/10.1021/am4001634.

[22] W. Zhao, X. Zhou, Z. Xue, B. Wu, X. Liu, X. Lu, Electrodeposition of platinum nanoparticles on polypyrrole-functionalized graphene, J. Mater. Sci. 48 (2013) 2566–2573, http://dx.doi.org/10.1007/s10853-012-7047-1.

[23] X. Zuoa, Y. Zhanga, L. Sia, B. Zhoua, B. Zhaoa, L. Zhub, X. Jianga, One-step electrochemical preparation of sulfonated graphene/polypyrrole composite and its application to supercapacitor, J. Alloys Compd. 688B (2016) 140–148, http://dx.doi.org/10.1016/j.jallcom.2016.07.184.

[24] H. Zhang, Z. Hu, M. Li, L. Hu, Sh. Jiao, A high-performance supercapacitor based on a polythiophene/multiwalled carbon nanotube composite by electropolymerization in an ionic liquid microemulsion, J. Mater. Chem. A 2 (2014) 17024–17030, http://dx.doi.org/10.1039/c4ta03369h.

[25] A. Takahashi, C.J. Lin, K. Ohshimizu, T. Higashihara, W.C. Chen, M. Ueda, Synthesis and characterization of novel polythiophenes with graphene-like structures via intermolecular oxidative coupling, Polym. Chem. 3 (2012) 479–485, http://dx.doi.org/10.1039/c1py00501d.

[26] S. Mondal, U. Rana, S. Malik, Graphene quantum dot-doped polyanilinenanofiber as high performance supercapacitor electrode materials, Chem. Commun. 51 (2015) 12365–12368, http://dx.doi.org/10.1039/C5CC03981A.

[27] K. Zhang, L.L. Zhang, X. Zhao, J. Wu, Graphene/polyaniline nanofiber composites as supercapacitor electrodes, Chem. Mater. 22 (2010) 1392–1401, http://dx.doi.org/10.1021/cm902876u.

[28] X.M. Feng, R.M. Li, Y.M. Ma, R.F. Chen, N.E. Shi, Q.L. Fan, W. Huang, One-step electrochemical synthesis of graphene/polyaniline composite film and its applications, Adv. Funct. Mater. 21 (2011) 2989–2996, http://dx.doi.org/10.1002/adfm.201100038.

[29] J. Yan, T. Wei, B. Shao, Z. Fan, W. Qian, M. Zhang, F. Wei, Preparation of a graphene nanosheet/polyaniline composite with high specific capacitance, Carbon 48 (2010) 487–493, http://dx.doi.org/10.1016/j.carbon.2009.09.066.

[30] J. Yan, T. Wei, Z. Fan, W. Qian, M. Zhang, X. Shen, F. Wei, Preparation of graphene nanosheet/carbon nanotube/polyaniline composite as electrode material for supercapacitors, J. Power Sources 195 (2010) 3041–3045, http://dx.doi.org/10.1016/j.jpowsour.2009.11.028.

[31] B.N. Liu, F. Luo, H. Wu, Y. Liu, Ch. Zhang, J. Chen, One-step ionic-liquid-assisted electrochemical synthesis of ionic-liquid-functionalized graphene sheets directly from graphite, Adv. Funct. Mater. 18 (2008) 1518–1525, http://dx.doi.org/10.1002/adfm.200700797.

[32] M. Matsumoto, Y. Saito, C. Park, T. Fukushima, T. Aida, Ultrahigh-throughput exfoliation of graphite into pristine 'single-layer' graphene using microwaves and molecularly engineered ionic liquids, Nat. Chem. 7 (2015) 730–736, http://dx.doi.org/10.1038/nchem.2315.

[33] G. Zotti, S. Cattarin, N. Comisso, Electrodeposition of polythiophene, polypyrrole and polyaniline by the cyclic potential sweep method, J. Electroanal. Chem. 235 (1987) 259–273, http://dx.doi.org/10.1016/0022-0728(87)85212-9.

[34] K. Sasaki, M. Kaya, J. Yano, A. Kitani, A. Kunai, Growth mechanism in the electropolymerization of aniline and p-aminodiphenylamine, J. Electroanal. Chem. 215 (1986) 401–407, http://dx.doi.org/10.1016/0022-0728(86)87033-4.

[35] S.Q. Jiao, J.G. Tu, C.Y. Fan, J.G. Hou, D.J. Fray, Electrochemically assembling of a porous nano-polyaniline network in a reverse micelle and its application in a supercapacitor, J. Mater. Chem. 21 (2011) 9027–9030, http://dx.doi.org/10.1039/c1jm11064k.

[36] D. Saini, T. Basu, Synthesis and characterization of nanocomposites based on polyaniline-gold/graphene nanosheets, J. Appl. Nanosci. 2 (2012) 467–479, http://dx.doi.org/10.1007/s13204-012-0059-y.

[37] J. Wu, Q. Tang, Q. Li, J. Lin, Self-assembly growth of oriented polyaniline arrays: a morphology and structure study, Polymer 49 (2008) 5262–5267, http://dx.doi.org/10.1016/j.polymer.2008.09.044.

[38] Q. Tang, J. Wu, X. Sun, Q. Li, J. Lin, L. Fan, Polyacrylamide-controlled growth of centimeter-scaled polyaniline fibers, Polymer 50 (2009) 752–755, http://dx.doi.org/10.1016/j.polymer.2008.11.052.

[39] M. Baibarac, I. Baltog, C. Godon, S. Lefrant, O. Chauvet, Covalent functionalization of single-walled carbon nanotubes by aniline electrochemical polymerization, Carbon 42 (2004) 3143–3152, http://dx.doi.org/10.1016/j.carbon.2004.07.030.

[40] Ch.F. Chang, Q.D. Truong, J.R. Chen, Graphene sheets synthesized by ionic-liquid-assisted electrolysis for application in water purification, Appl. Surf. Sci. 264C (2013) 329–334, http://dx.doi.org/10.1016/j.apsusc.2012.10.022.
[41] M. Sawangphruk, M. Suksomboon, K. Kongsupornsak, J. Khuntilo, P. Srimuk, Y. Sanguansak, P. Klunbud, Ph. Suktha, P. Chiochan, High-performance supercapacitors based on silver nanoparticle–polyaniline–graphene nanocomposites coated on flexible carbon fiber paper, J. Mater. Chem. A 1 (2013) 9630–9636, http://dx.doi.org/10.1039/c3ta12194a.
[42] A. Petrovski, P. Paunovic, R. Avolio, M. Errico, M. Cocca, G. Gentile, A. Grozdanov, M. Avella, J. Barton, A. Dimitrov, Synthesis and characterization of nanocomposites based on pani and carbon nanostructures prepared by electropolymerization, J. Mat. Chem. Phys. 185 (2016) 83–90, http://dx.doi.org/10.1016/j.matchemphys.2016.10.008.
[43] H. Yu, T. Wang, B. Wen, M. Lu, Zh. Xu, Ch. Zhu, Y. Chen, X. Xue, Ch. Sun, M. Cao, Graphene/polyaniline nanorod arrays: synthesis and excellent electromagnetic absorption properties, J. Mater. Chem. 22 (2012) 21679–21685, http://dx.doi.org/10.1039/c2jm34273a.
[44] D.W. Wang, F. Li, J.P. Zhao, W.C. Ren, Z.G. Chen, J. Tan, Z.Sh. Wu, I. Gentle, G.Q. Lu, H.M. Cheng, Fabrication of graphene/polyaniline composite paper via in situ anodic electropolymerization for high-performance flexible electrode, ACS Nano 3 (2009) 1745–1752, http://dx.doi.org/10.1021/nn900297m.
[45] L. Hu, J. Tu, Sh. Jiao, J. Hou, H. Zhu, D.J. Fray, In situ electrochemical polymerization of a nanorod-PANI–Graphene composite in a reverse micelle electrolyte and its application in a supercapacitor, Phys. Chem. Chem. Phys. 14 (2012) 15652–15656, http://dx.doi.org/10.1039/c2cp42192e.
[46] Z.X. Zheng, Y.L. Du, Q.L. Feng, Z.H. Wang, C.M. Wang, Facile method to prepare Pd/graphene–Polyaniline nanocomposite and used as new electrode material for electrochemical sensing, J. Mol. Catal. A Chem. 353 (2012) 80–86, http://dx.doi.org/10.1016/j.molcata.2011.10.027.
[47] L.L. Zhang, S. Li, J.T. Zhang, P.Z. Guo, J.T. Zheng, X.S. Zhao, Enhancement of electrochemical performance of macroporous carbon by surface coating of polyaniline, Chem. Mater. 22 (2010) 1195–1202, http://dx.doi.org/10.1021/cm902685m.
[48] S.W. Woo, K. Dokko, H. Nakano, K. Kanamura, Incorporation of polyaniline into macropores of three-dimensionally ordered macroporous carbon electrode for electrochemical capacitors, J. Power Sources 190 (2009) 596–600, http://dx.doi.org/10.1016/j.jpowsour.2009.01.050.
[49] Q. Wu, Y.X. Xu, Z.Y. Yao, A.R. Liu, G.Q. Shi, Supercapacitors based on flexible graphene/polyaniline nanofiber composite films, ACS Nano 4 (2010) 1963–1970, http://dx.doi.org/10.1021/nn1000035.
[50] H. Zhang, G. Cao, Z. Wang, Y. Yang, Z. Shi, Z. Gu, Tube-covering-tube nanostructured polyaniline/carbon nanotube array composite electrode with high capacitance and superior rate performance as well as good cycling stability, Electrochem. Commun. 10 (2008) 1056–1059, http://dx.doi.org/10.1016/j.elecom.2008.05.007.
[51] C. Kim, K.S. Yang, Electrochemical properties of carbon nanofiber web as an electrode for supercapacitor prepared by electrospinning, Appl. Phys. Lett. 83 (2003) 1216–1218, http://dx.doi.org/10.1063/1.1599963.
[52] T. Li, M. Beidaghi, X. Xiao, L. Huang, Z. Hu, W. Sun, X. Chen, Y. Gogotsi, J. Zhou, Ethanol reduced molybdenum trioxide for Li ion capacitors, Nano Energy 26 (2016) 100–107, http://dx.doi.org/10.1016/j.nanoen.2016.05.004.
[53] X.S. Du, M. Xiao, Y.Z. Meng, Synthesis and characterization of polyaniline/graphite, J. Appl. Polym. Sci. Part B Polym. Phys. 42 (2004) 1972–1978, http://dx.doi.org/10.1002/polb.20102.